doi:10.3772/j.issn.1006-6748.2021.03.005

Research on gas leakage through suction valves of reciprocating compressor under varying load conditions①

Zhang Jinjie (张进杰)**, Wang Yao②**, Zhang Chun*, Jiang Zhinong**, Sun Xu*
(*Compressor Health and Intelligent Monitoring Center of National Key Laboratory of Compressor Technology, Beijing University of Chemical Technology, Beijing 100029, P. R. China)
(**Beijing Key Laboratory of Health Monitoring Control and Fault Self-Recovery for High-End Machinery, Beijing University of Chemical Technology, Beijing 100029, P. R. China)

Abstract

A research concerning the coupling conditions of gas leakage through suction valves and capacity regulation is performed in an industrial reciprocating compressor. Both internal flow and thermodynamic characteristic are discussed in detail. The results show that the capacity of compressor can be regulated steplessly by controlling suction valve closure moment. And then the quantitative relationship between the capacity load and the closing angle of suction valve is revealed. The capacity load and valve leakage rate show obvious different features in P-V diagrams, which makes it easier to define appropriate features for detecting cracked or broken reciprocating compressor valves under varying load conditions. A set of curves of compression work and discharge gas mass are obtained and a method for rating thermal performance of a compressor is presented using these curves.

Key words: reciprocating compressor, computational fluid dynamics (CFD), variable load, suction valve leakage, thermal performance

0 Introduction

Reciprocating compressors are widely used in petroleum, chemical, fertilizer, natural gas transportation, refrigeration field, etc. On one hand, when the production demand changes, for example, the production process changes the demand of compressor displacement or change of the suction source gas capacity, requires the function of exhaust capacity control. Top opening suction valve adjustment is a typical adjustment method[1-2]. On the other hand, gas valve failures of reciprocating compressors occur frequently, resulting in reduced unit efficiency and even accidents.

Various methods have been proposed for the research of reciprocating compressors[3-5], depending on the level of details needed and aspects focused on. Becaues the computational fluid dynamics (CFD) analyses of compressors can give the most detailed characterization of compressor performances, CFD technology is widely used in numerical research of compressors. Ref. [6] described a two-dimensional CFD modeling strategy and analyzed the numerical simulation of the thermodynamic cycle of large reciprocating compressors. Ref. [7] used the fluid solid interaction (FSI) model to study the delayed shutdown of the refrigeration compressor suction valve.

Leakage of suction valves is a very common defect that affects compressor operation and reduces compressor performance and effectiveness. Ref. [8] carried out research of valve fault decetion for single-stage reciprocating compressors. Ref. [9] proposed the model of gas leakage through compressor valves. The large amount and variety of researches have shown that it is very important to detect and diagnose valve faults in reciprocating compressors[10-12].

Mathematical models have been proposed to simulate the reciprocating compressor gas capacity regulation conditions. Ref. [13] used mathematical models to simulate the reciprocating compressor gas capacity regulation conditions and optimize system control and execution of structural motion parameters. Ref. [14] analyzed the thermal cycle for the basic principle of the large-scale reciprocating compressor stepless capacity

① Supported by the National Natural Science Foundation of China (No. 52101343), and State Key Laboratory of Compressor Technology (An Hui Laboratory of Compressor Technology) (No. SKL-YSJ201808/SKL-YSJ201911).
② To whom correspondence should be addressed. E-mail: wyaobeijing@163.com
Received on June 3, 2020

control system. Refs[15,16] combined the mathematical model of compressor to explore the effect of actuator and hydraulic system on compressor performance under gas capacity regulation conditions. Mathematical models are generally fast to calculate but can't get flow details.

Above all, most of the research reports focus on the study of the single operating condition of reciprocating compressors. There are few studies on the coupling conditions of gas leakage through suction valves and capacity regulation of industrial reciprocating compressors.

In order to optimize the response characteristics of the gas capacity regulation system actuator, effectively diagnose the valve leakage failure, and accurately analyze the energy consumption of the compressor, a 3D CFD model of a double-acting reciprocating compressor is built to study the effect at the exhaust capacity control mode.

Firstly, the valve plate was controled by unloader to realize the simulation of the gas capacity regulation condition. The experimental tests under various load conditions were completed. The simulation model was validated through the comparison analysis of the experimental and simulation data. The relationship between the closure angle of the suction valve and the capacity load under the gas capacity regulation condition was obtained. Then, the suction valve rupture model was used to simulate the suction valve leakage failure. Based on this, the situation was simulated where the suction valve leaked when the compressor capacity load changed. Finally, the internal flow field variables of the cylinder under the leakage and coupling conditions, the compressor leakage amount, the suction valve closure angle and the energy consumption were analyzed, and the conclusion was drawn.

1 Numerical model

Nomenclature in this paper is listed on Table 1.

Table 1 Nomenclature

q	internal heat source	q	heat flux density
ρ	density	T	temperature
U, $\boldsymbol{U}$	speed, plus black as vector	$-(2/3)\mu S_{kk}\delta_{ij}$	isotropic viscous stress
$T_{ij}e_ie_j$	surface stress tensor	$2\mu S_{ij}$	bias stress tensor
$\boldsymbol{f}$	volume force	Ω	volume
λ	thermal conductivity	Σ	surface
P	pressure	$\boldsymbol{P}_1$	the upper surface pressure of the valve plate
$-p\delta_{ij}$	thermodynamic	$\boldsymbol{P}_2$	the lower surface pressure of the valve plate
$\boldsymbol{G}$	gravity	$\boldsymbol{F}_1$	spring force
$Q(f)$	compressor exhaust at full load	$\boldsymbol{F}_2$	liquid pressure
$Q(r)$	compressor real exhaust	k	spring stiffness
$Q(c)$	compressor exhaust at controlled load		

In order to study the thermodynamic performance of the compressor and the operating state of the valve, the computational fluid dynamics software Fluent based on the finite volume method is used to calculate. RNG k-ε model was selected as turbulence model[17].

1.1 Control equations and boundary conditions

Any flow problem is governed by the three conservation laws of mass, momentum, and energy. The expressions are as follows.

$$\frac{\partial \rho}{\partial t} + \nabla \cdot (\rho \boldsymbol{U}) = 0 \tag{1}$$

$$\frac{\partial (\rho \boldsymbol{U})}{\partial t} + \nabla \cdot (\rho \boldsymbol{U}\boldsymbol{U}) = \rho \boldsymbol{f} + \nabla \cdot (T_{ij}\boldsymbol{e}_i\boldsymbol{e}_j) \tag{2}$$

$$\frac{\partial}{\partial t}\left[\rho\left(e + \frac{\boldsymbol{U}^2}{2}\right)\right] + \nabla \cdot \left[\rho\left(e + \frac{\boldsymbol{U}^2}{2}\right)\boldsymbol{U}\right] = \rho \boldsymbol{f} \cdot \boldsymbol{U} + \nabla \cdot (\boldsymbol{U} \cdot T_{ij}\boldsymbol{e}_i\boldsymbol{e}_j) + \rho q + \lambda \Delta T \tag{3}$$

The compressed medium was air and the gas model was selected as the ideal gas[18-19].

The calculation domain is shown in Fig. 1.

According to the working parameters of the compressor, the initial conditions and boundary conditions were set. The initial conditions of the inlet boundary to the upper surface of the suction valve Ω_1 and the cylinder watershed $\Omega_{2\text{-}2}$ are the suction temperature and the suction pressure, respectively. The initial condition of the initial clearance flow area, $\Omega_{2\text{-}1}$, and the initial conditions of the watershed between the lower surface of the exhaust valve and the outlet boundary, i.e.,

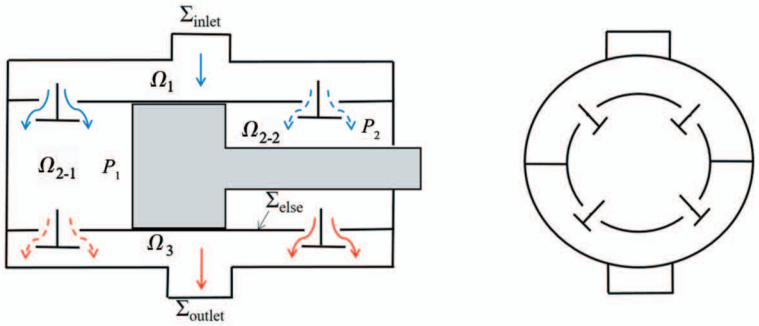

Fig. 1 Schematic diagram of the calculation domain (not to scale)

Ω_3, are the exhaust temperature and the exhaust pressure, and the specific values were measured by the sensor.

The unsteady flow initial field was determined by the calculation domain.

$$\begin{cases} t = 0: \\ U = U(\Omega_1 + \Omega_{2-1} + \Omega_{2-2} + \Omega_3, t_0) \\ P = P(\Omega_1 + \Omega_{2-1} + \Omega_{2-2} + \Omega_3, t_0) \\ T = T(\Omega_1 + \Omega_2 - 2 + \Omega_2 - 1 + \Omega_3, t_0) \end{cases} \tag{4}$$

$$\begin{cases} U(\Omega_1 + \Omega_{2-1} + \Omega_{2-2} + \Omega_3, t_0) = 0 \\ P = P(\Omega_{2-1} + \Omega_3, t_0) = 280\ \text{kPa} \\ P = P(\Omega_1 + \Omega_{2-2}, t_0) = 0\ \text{kPa} \\ T = T(\Omega_{2-1} + \Omega_3, t_0) = 395\ \text{K} \\ T = T(\Omega_1 + \Omega_{2-2}, t_0) = 300\ \text{K} \end{cases} \tag{5}$$

Boundary conditions are given by

$$\begin{cases} P(\Sigma_{inlet}) = 101.325\ \text{kPa} \\ P(\Sigma_{outlet}) = 280\ \text{kPa} \\ T(\Sigma_{inlet}) = 300\ \text{K} \\ T(\Sigma_{outlet}) = 395\ \text{K} \end{cases} \tag{6}$$

$$q(\Sigma_{else}) = 0 \tag{7}$$

where Σ_{inlet} is the inlet condition for the suction pressure and the suction temperature, Σ_{outlet} is the outlet condition for the exhaust pressure and the exhaust temperature. Except for the boundary other than the inlet and outlet, the remaining boundary Σ_{else} is adiabatic solid wall, the fluid velocity is consistent with the local wall velocity, and the heat flux density is zero. The calculation of near-wall flow adopts the standard wall function method.

1.2 Physical geometry and computational domain dispersion

A three-dimensional model was proposed to analyze the performance of the DW12-2 reciprocating compressor under varying load conditions. The computational domain modeling and its discrete grid are shown in Fig. 2. Grid refinement was performed in different regions. When the element size of the valve, cylinder, and air chamber is about 0.001 m, 0.002 m, and 0.004 m, the calculation results meet the grid independence requirements.

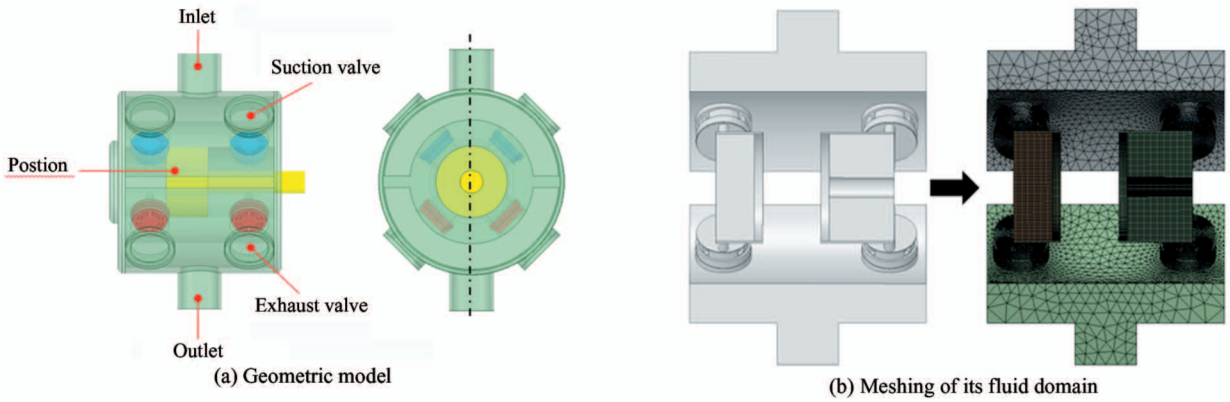

Fig. 2 The geometric model of reciprocating compressor and meshing of its fluid domain

1.3 Valve motion principle and valve failure type

Compressor structure and operating parameters are shown in Table 2.

The leakage rate of a single valve is calculated as

$$Ra = \frac{Av}{A_F} \times 100\% \tag{8}$$

where A_F is leakage flow area of the suction valve plate and A_v is valve gap flow area.

The structure of the suction and exhaust valve of

the compressor is a mesh valve. The structure of the valve after adding the ejector is shown in Fig. 3.

Fig. 4 shows the suction valve plate model under different fracture degrees and the mesh processing of the leakage flow area.

Table 2 Structural size of the compressor and valve part

Parameter name	Value
Link length ι/m	0.45
Crankshaft radius r/m	0.09
Rated speed n/r/min	495
Valve stroke/mm	2
Valve thickness/mm	1.2
Valve gap flow area A_V/mm^2	2675.24

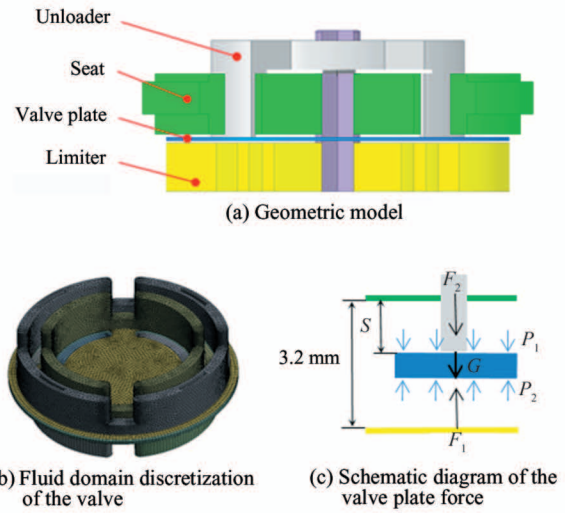

Fig. 3 Structure and fluid domain of a plate valve

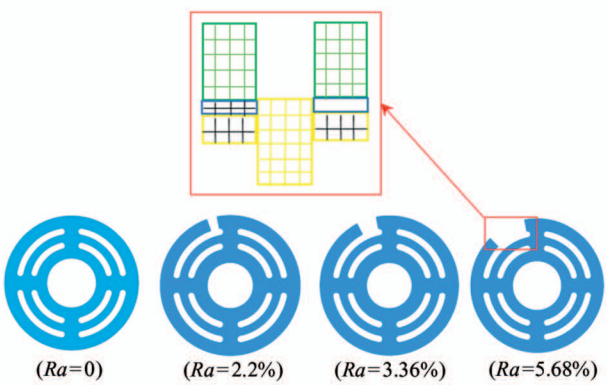

Fig. 4 Valve fracture model and leakage flow region discretization

The movement of the valve plate was approximated as a single-degree-of-freedom linear motion. The force equation of the suction valve is expressed as follows.

$$m\frac{\mathrm{d}^2\boldsymbol{S}}{\mathrm{d}t^2} = \boldsymbol{G} + \boldsymbol{P}_1 + \boldsymbol{P}_2 + \boldsymbol{F}_1 + \boldsymbol{F}_2 \tag{9}$$

$$F_1 = k(S + S_0) \tag{10}$$

The speed reversed after a rebound occured during the movement of the valve plate. The ratio C_R of the current speed V_{tem} to the rebound speed V_{rec} was the rebound coefficient of empirical value 0.2.

$$V_{rec} = -C_R \times V_{tem} \tag{11}$$

1.4 Calculation flowchart and convergence criteria

The determination condition for stopping the calculation is the convergence criterion. The setting of convergence criteria for different flow processes is artificially determined according to different accuracy requirements. Ref. [17] used the pressure of the buffer tank and the inlet and outlet mass flow as convergence criteria. Ref. [20] used two iterations between the maximum pressure difference and the temperature difference at the same crank angle position as less than the set tolerance as a convergence criterion. It has been found that the sensitivity of temperature changes is high based on previous simulation experience. Therefore, the convergence criterion is set using the average temperature of the gas in the cylinder. Of course, this is not the only setting criterion. Other flow variables can also be chosen to set the convergence criterion, as long as the required simulation accuracy is met. The convergence criterion is that the maximum average temperature difference of gas in the cylinder between the two iterations at the same crank angle location is less than the set tolerance 0.01. The variation law of the average temperature of the gas in the cylinder with the calculation cycle is shown in Fig. 5.

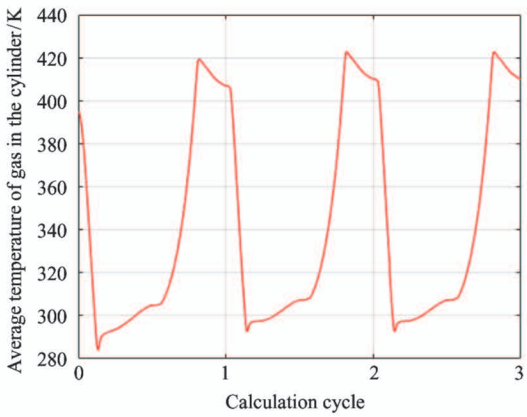

Fig. 5 Temperature curves in the cylinder within the 3 cycles

The valve movement was controlled by a custom function. The valve motion chart is shown in Fig. 6.

The principle of the motion control of the exhaust valve is similar to that of suction valve, except that there is no hydraulic force $\boldsymbol{F}_2$ during its movement. The movement of the piston was set by Fluent cylinder model.

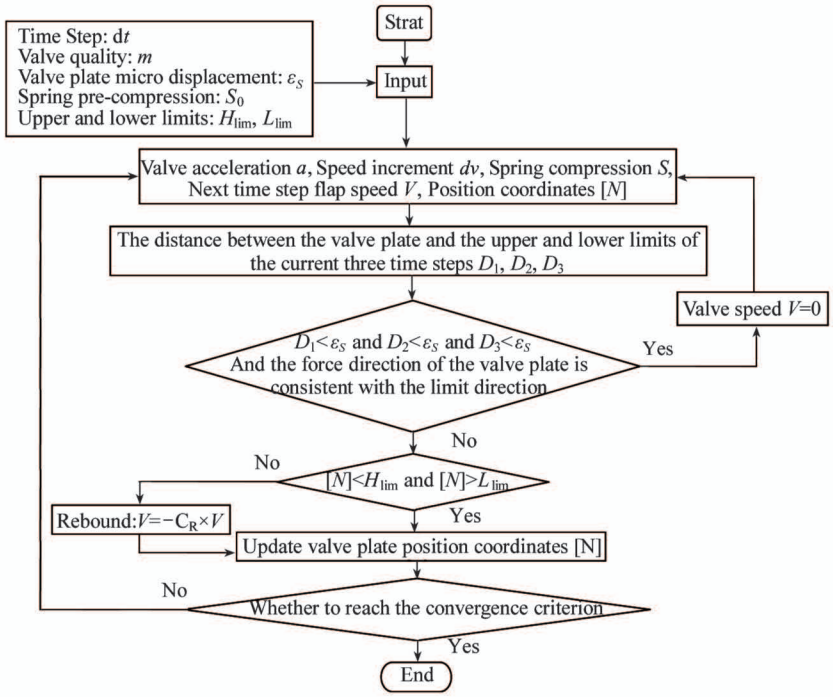

Fig. 6 Valve plate motion control flow chart

Fig. 7 illustrates the movement of the crankshaft connecting rod mechanism, and also shows the $\boldsymbol{F}_2$ acting in the phase angle φ interval, and the closing phase of the suction valve.

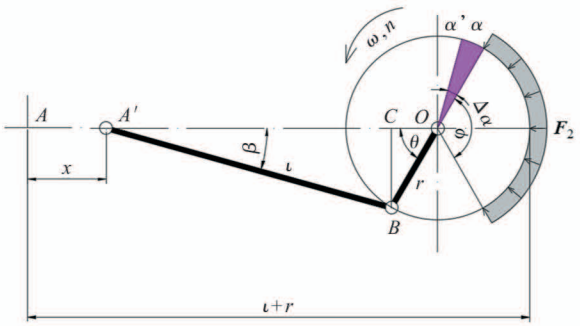

Fig. 7 Crankshaft linkage motion diagram

The curve of piston displacement with crankshaft angle θ can be described as (if $\iota \geqq 5r$)

$$X = r(1 - \cos\theta) + \iota(1 - \cos\beta)$$
$$\approx r\left[(1 - \cos\theta) + \frac{r}{4\iota}(1 - \cos 2\theta)\right] \quad (12)$$

$$Q(c) = \left(1 - \frac{X}{2r}\right) \times Q(f) \quad (13)$$

Suction valve closure time is

$$\Delta t = \frac{\Delta\alpha}{360n} \quad (14)$$

The hydraulic force $\boldsymbol{F}_2$ acts on the valve sealing element after the valve plate opens during the suction phase. η and η' represent the nominal load ratio and the actual load ratio, respectively.

$$\eta = \frac{Q(c)}{Q(f)},\ \eta' = \frac{Q(r)}{Q(f)} \quad (15)$$

Among them, $\eta = 100\%$ means that the closure of the valve plate is not affected by $\boldsymbol{F}_2$. As the closing angle of the suction valve is delayed, the displacement gas volume decreased, thereby realizing the regulation of the compressor gas capacity.

2 Experimental setup

2.1 Measurement of the parameters

Fig. 8 shows the reciprocating compressor experimental platform with hydraulic stepless gas capacity regulation system and pressure sensor (WIKA S-10), arrangement. The compressor is driven by a motor, and the cooling method is water circulation cooling. The net weight of the compressor is 3000 kg; the shaft power is not more than 41 kW; length, width and height are 3670 mm, 1270 mm, and 750 mm. To accurately measure

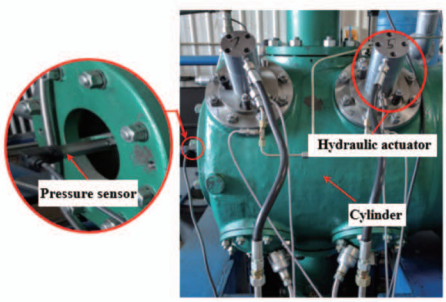

Fig. 8 Reciprocating compressor experimental platform

valve displacement, a new valve structure was designed with an eddy current sensor (Bently 3300XL) embedded in the valve seat, as shown in Fig. 9. The sampling rate of the data acquisition system is 10 240 Hz.

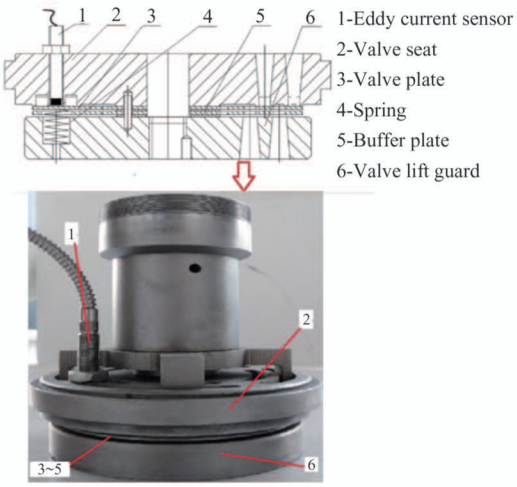

Fig. 9 Arrangement of eddy current sensor

2.2 Experimental condition

During the experimental test, it is necessary to control the compressor to run stably, stabilize the exhaust pressure, adjust the compressor capacity load to be stable, and read the experimental data that the suction valve is closed at different angles.

3 Simulation and analysis

3.1 Comparison of measured and predicted results of capacity regulation conditions

The method adjusting capacity by controlling suction valve can realize the stepless capacity regulation because it keeps the valve plate open during some certain running moments.

Fig. 10 displays the plot for the measured and predicted valve displacement and cylinder pressure as a function of the crankshaft angle, obtained in a complete compressor work cycle under four capacity loads.

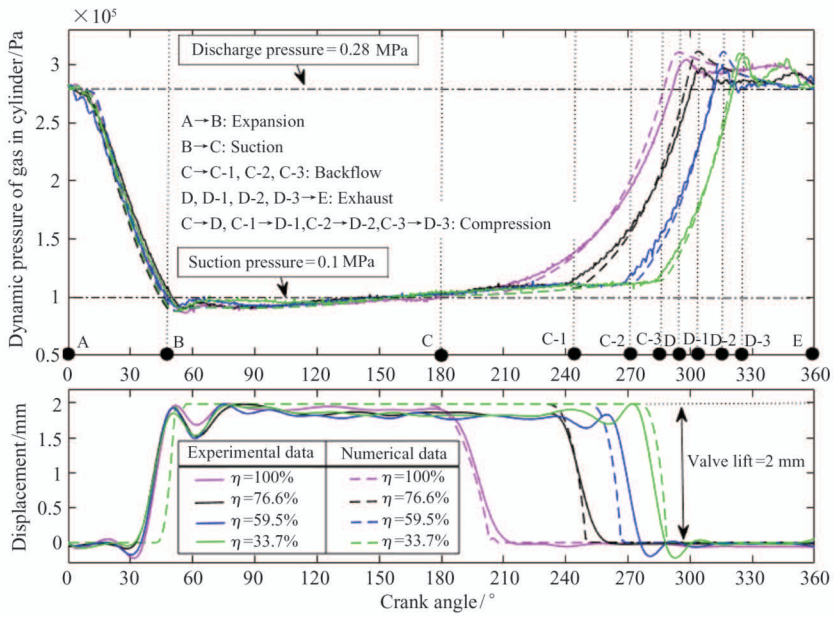

Fig. 10 Comparison of numerical data and experimental data of dynamic pressure and displacement of suction valve

As clearly displayed in Fig. 10, the closing process of the suction valve plate and the subsequent compression stroke are delayed with the reduction in capacity load. As the duration of the discharge time shortens, the gas output capacity is continuously reduced. The experimental data of the displacement of the suction valve plate flap is more severe than the numerical data, and the experimental pressure of the exhaust phase has more obvious fluctuations than the numerical data, which may be due to the fact that the suction and exhaust tank are ignored in the simulation.

The calculation results and the measured results are compared. Fig. 11 shows the results. It is clear that the calculated cylinder pressure under different capacity loads fits well to the measured values while the maximum errors are smaller than 10%.

3.2 Analysis of the influence of the capacity regulation on compressor performance

The effect of capacity regulation on the thermodynamic performance of the compressor was further explored.

As shown in Fig. 12, the average temperature of the cylinder gas before the compression increased as

the capacity declined. One reason for the rise of temperature was increased backflow resistance loss through the suction valve. On the other hand, this also provides support for the proposed optimal design of the suction valve under the condition of gas capacity regulation.

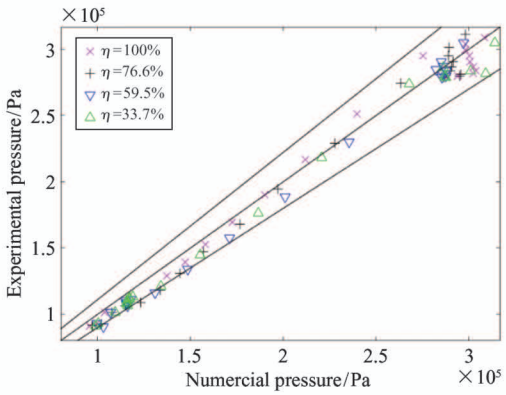

Fig. 11 Calculated vs measured cylinder pressure under different loads

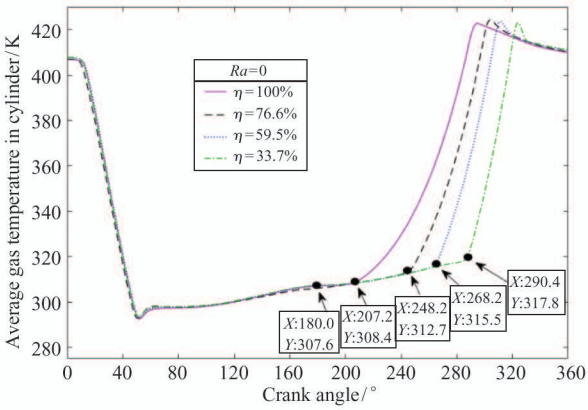

Fig. 12 Average gas temperature in the cylinder

Fig. 13 shows the gas mass varies in the cylinder under the gas capacity regulation conditions.

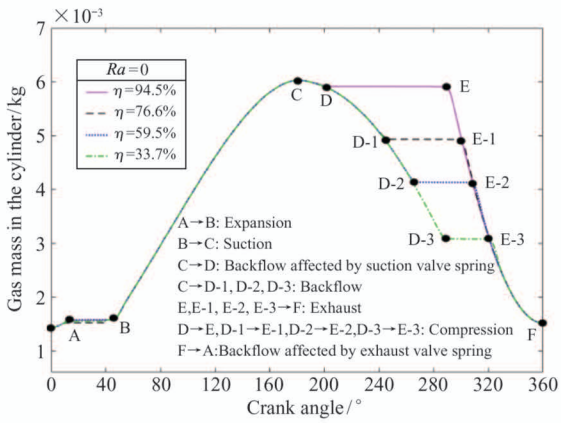

Fig. 13 Variation in gas mass in the cylinder

According to Fig. 13, the actual compressed air volume of the compressor clearly decreases as the capacity declines. The method of adjusting capacity by controlling suction valve closure moment can realize the stepless capacity regulation because it controls the valve plate during all the running moments.

When the piston moves reversely from the piston position of BCD, all suction valves are still held open under capacity regulation conditions.

This article assumed that the actuator was retracted fast enough and the valve plate withdrawal was only affected by the air flow. It can be seen from Fig. 14 that when the suction valve is closed at different angles, the closing time is different.

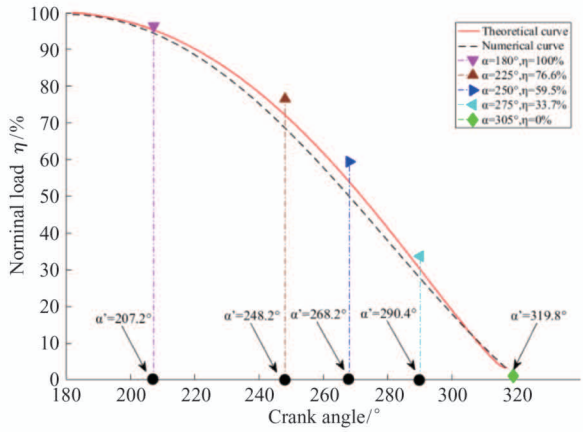

Fig. 14 The relationship between the capacity load and the crank angle

The suction valve closing time under different loads is shown in Fig. 15. When η reached 59.5%, the piston movement accelerated, which caused the valve plate to withdraw faster.

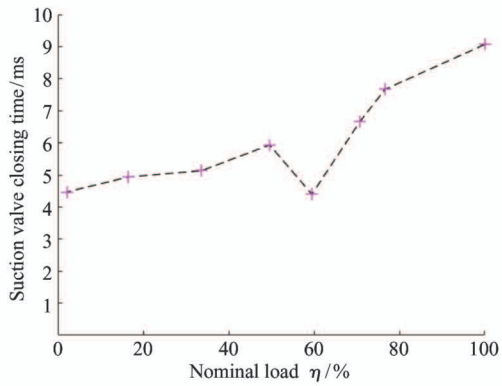

Fig. 15 Power diagram under suction valve leak conditions

3.3 Dynamic pressure change of gas in the cylinder under leakage conditions

Fig. 16 shows the P-V diagrams of the compressor for different leakage rates when capacity load η = 59.5%. Under normal operating condition, the shape

of P-V diagram is only determined by capacity regulation. There is one-to-one correspondence between capacity load and the end moment of backflow process (point D in Fig. 16).

Under valve leakage conditions, the decline rate of cylinder pressure during the expansion process increases compared with normal operating condition. And the larger the valve leakage rate is, the quicker the cylinder pressure declines and therefore the slower the gas is compressed during compression process.

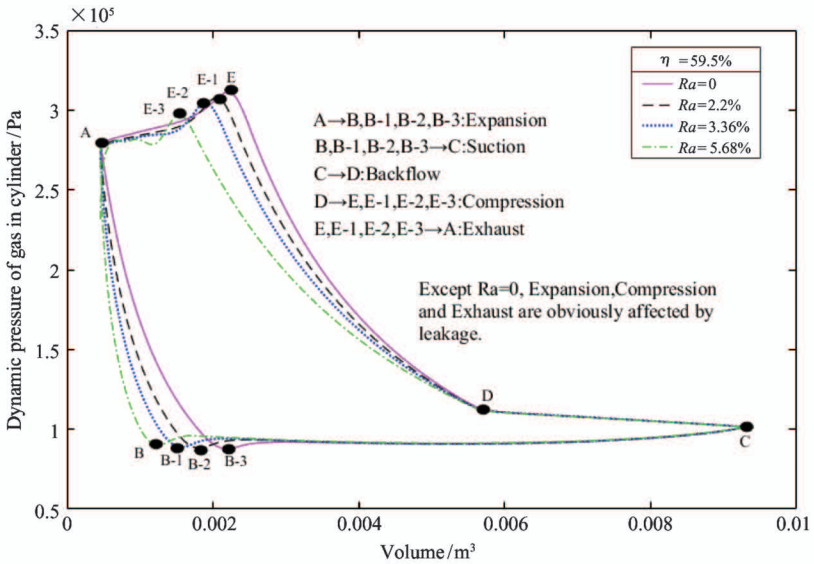

Fig. 16 Power diagram under suction valve leak conditions

In view of the above, the decline rates of cylinder pressure during both the expansion and compression processes and the end moment of backflow process can be used as distinguishing characteristics of valve leakage under capacity regulation conditions.

Table 3 shows the indicated power and valve power loss under the leakage condition in Fig. 16 for detail.

Table 3 Indicated power and power loss through valves

Ra	Indicated power/J	Suction/J	Discharge/J
0	657.80	65.81	30.84
2.20%	614.86	68.03	22.02
3.36%	606.34	68.20	15.99
5.68%	571.98	65.98	5.96

3.4 Performance curve of compressor under coupling conditions of valve leakage and capacity regulation

A set of curves of compression work and discharge gas mass for a single cycle of a compressor's single-side cylinder were obtained, as shown in Fig. 17. Least square method was used to fit compressor characteristic curve coupling conditions of valve leakage and capacity regulation. When the capacity load is 100%, the compression work and gas mass descends along with the curve A-B in Fig. 17 with the increase of valve leakage rate *Ra*. The output gas mass reduces to zero when valve leakage rate reaches 6.8%. As valve leakage rate continues to increase, the compression work of compressor decreases along the curve B-C.

If there is no leakage, the compression work and gas mass are only determined by capacity load. Performance curve of compressor under capacity regulation is shown as the curve C-A in Fig. 17. The compression work and gas mass increase as the capacity load rises from 0 to 100%. As shown in curve C-A, the power almost decreased linearly with capacity. When it reaches point C, the capacity reaches zero exactly, and this is called zero capacity point. The gas left in the cylinder cannot be compressed to the exhaust pressure under zero capacity load.

The triangle region in the graph surrounded by curves A-B, B-C and C-A is operating area of compressor under coupling conditions of valve leakage and capacity regulation. The actual working state of compressor could be obtained by the slope interpolation corresponding to the adjacent grid line.

Introduction to calibration methods, as shown by point E in Fig. 17, the compression power of a single cycle on one side of a single cylinder is 600 J and the discharge mass is 0.001 kg. Load interpolation from the slope of the curve corresponding to the adjacent condition $\eta = 59.5\%$ is equal to $\eta = 65.2\%$, and load interpolation from the slope of the curve corresponding to the adjacent condition $Ra = 5.68\%$ is equal to $Ra =$

4.91%. So far, the working state of the compressor under the suction valve leakage fault has been calibrated, so that the actual degree of failure (Ra = 4.91%) and capacity load deviation (η = 65.2%) can be determined.

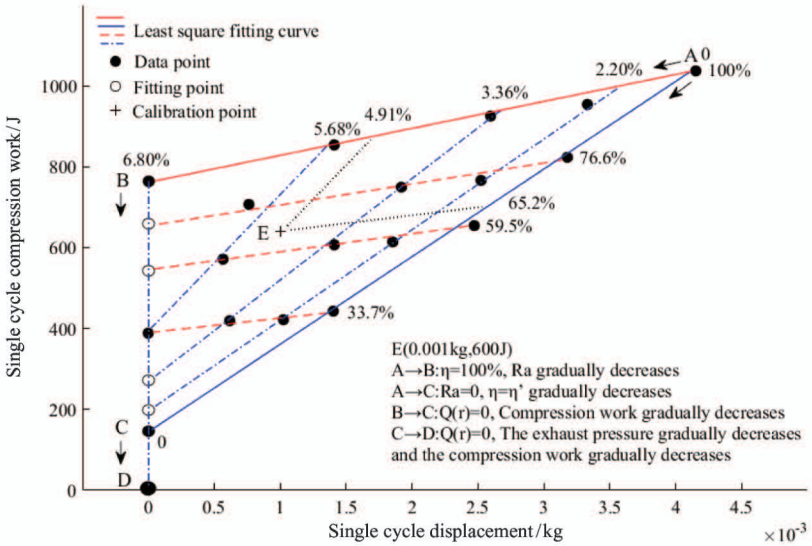

Fig. 17 Calibration curves of suction valve leakage and power consumption

3.5 Calculation domain pressure cloud diagram

Fig. 18 shows the pressure cloud diagrams of the calculation of the compressor at different times. At CA 5 °, an expansion wave was generated in the left cylinder near the middle surface of the high-pressure expansion cylinder. When CA 105 °, the pressure in the right cylinder was greater than the exhaust pressure. Since the compression wave was generated near the exhaust valve inside the exhaust cylinder, the expansion wave was generated near the piston. When CA 180 °, there was no obvious pressure wave. Finally, Fig. 19 shows the gas velocity and temperature distribution during a leak.

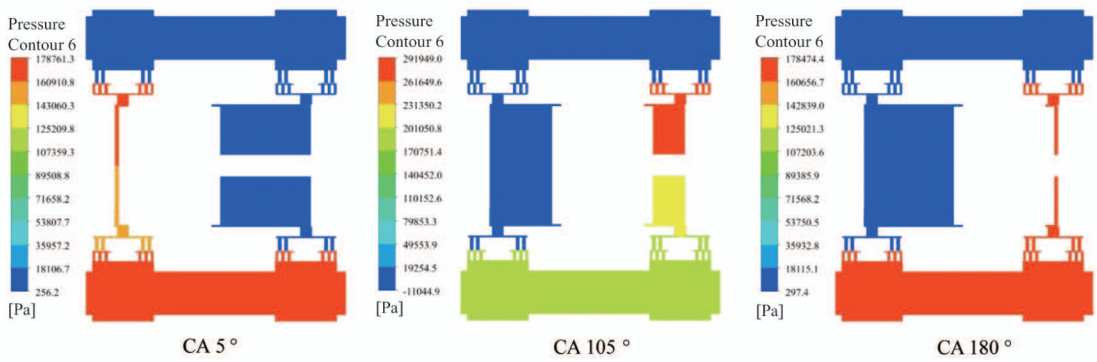

Fig. 18 Calculate the pressure map of the domain at different moments

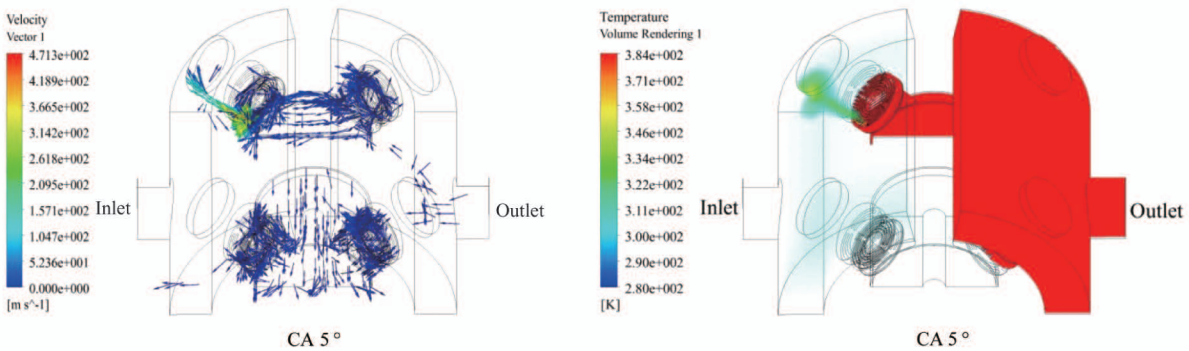

Fig. 19 Speed vector diagram and temperature cloud diagram display under leakage conditions

4 Conclusions

In this paper, the thermal performance of an air compressor under coupling conditions of valve leakage and capacity regulation has been studied by CFD model and experiment. The capacity of compressor can be regulated steplessly by controlling suction valve closure moment. The curves indicating relationship between capacity load and the closing angle of suction valve are presented. The temperature of the cylinder gas before the compression increased from 307.6 K to 317.8 K as the capacity declined from 100% to 33.7%. The valve leakage rate significantly impacts the slope of the expansion and compression curves in P-V diagram while capacity load has an impact on backflow curves. A set of curves of compression work and discharge gas mass are obtained and a method for rating thermal performance of a compressor is presented using these curves.

References

[1] Li D C, Wu H Q, Gao J J. Experimental study on stepless capacity regulation for reciprocating compressor based on novel rotary control valve[J]. *International Journal of Refrigeration*, 2013, 36: 1701-1715

[2] Wang Y, Zhang J J, Zhou C, et al. Study on effect analysis and parameter optimizing of stepless capacity control system on reciprocating compressors[J]. *High Technology Letters*, 2018, 24(1): 1-9

[3] Elhaj M, Gu F, Ball A D, et al. Numerical simulation and experimental study of a two-stage reciprocating compressor for condition monitoring[J]. *Mechanical Systems and Signal Processing*, 2008, 22: 374-389

[4] Roland A, Herbert S. Modelling fluid dynamics, heat transfer and valve dynamics in a reciprocating compressor [C]//The 5th Conference of the EFRC, Prague, Czech, 2007: 171-180

[5] Volf M, Gášpár R. Modeling reciprocating compressors valves dynamics[C]//The 36th Meeting of Departments of Fluid Mechanics and Thermodynamics, Pilsen, Czech, 2017, 1889: 1-6

[6] Francesco B, Andrea T, Giovanni F, et al. Two-dimensional approach for the numerical simulation of large bore reciprocating compressors thermodynamic cycle[J]. *Applied Thermal Engineering*, 2018,129: 490-501

[7] Wang T, Yi G, He Z L, et al. Investigation on the delayed closure of the suction valve in the refrigerator compressor by FSI modeling[J]. *International Journal of Refrigeration*, 2018, 91: 111-121

[8] Mahmood F G, Hossein K. Valve fault decetion for single-stage reciprocating compressors[J]. *Journal of Natural Gas Science Engineering*, 2016, 35: 1239-1248

[9] Leandro R S, Cesar J D. Modeling of gas leakage through compressor valves[J]. *International Journal of Refrigeration*, 2015, 53: 195-205

[10] Tang H N, Yao H, Wang S J, et al. Numerical simulation of leakage rates of labyrinth seal in reciprocating compressor[C]//The 6th Global Conference on Materials Science and Engineering, Beijing, China, 2017: 1-8

[11] Wang Y F, Xue C, Jia X H, et al. Fault diagnosis of reciprocating compressor valve with the method integrating acoustic emission signal and simulated valve motion[J]. *Mechanical Sysrems and Signal Processing*, 2015, 56-57: 197-212

[12] Panagiotis L, George Z, Ian B, et al. Reciprocating compressor prognostics of an instantaneous failure mode utilising temperature only measurements[J]. *Applied Acoustics*, 2019, 147: 77-86

[13] Wang Y, Jiang Z N, Zhang J J, et al. Performance analysis and optimization of reciprocating compressor with stepless capacity control system under variable load conditions[J]. *International Journal of Refrigeration*, 2018, 94: 174-185

[14] Tang B, Zhao Y Y, Li L S, et al. Thermal performance analysis of reciprocating compressor with stepless capacity control system[J]. *Applied Thermal Engineering*, 2013, 54(2): 380-386

[15] Liu G B, Zhao Y Y, Tang B, et al. Dynamic performance of suction valve in stepless capacity regulation system for large-scale reciprocating compressor[J]. *Applied Thermal Engineering*, 2016, 96: 167-177

[16] Liu G B, Zhao Y Y, Wang L, et al. Dynamic performance of valve in reciprocating compressor used stepless capacity regulation system[C]//The 22nd International Compressor Engineering Conference at Purdue, West Lafayette, USA, 2014: 1-6

[17] Zhao B, Jia X H, Sun S K, et al. FSI model of valve motion and pressure pulsation for investigating thermodynamic process and internal flow inside a reciprocating compressor[J]. *Applied Thermal Engineering*, 2018, 131: 998-1007

[18] Peskin A P. The effects of different property models in a computational fluid dynamics simulation of a reciprocating compressor[J]. *International Journal of Thermophysics*, 1999, 20(1): 175-185

[19] Mahmood F G, Amir N, Mahdi D D, et al. Thermodynamic analysis of natural gas reciprocating compressors based on real and ideal gas models[J]. *International Journal of Refrigeration*, 2015, 56: 186-197

[20] Wang T, He Z L, Guo J, et al. Investigation of the thermodynamic process of the refrigerator compressor based on the m-θ diagram[J]. *Energies*, 2017, 10: 1-14

Zhang Jinjie, born in 1987. He received his Ph. D, M. S and B. S degrees from Beijing University of Chemical Technology. His research interests include reciprocating compressor fault diagnosis and stepless capacity controlling.